

Quantum transport of disordered Weyl semimetals at the nodal point

Björn Sbierski, Gregor Pohl, Emil J. Bergholtz, Piet W. Brouwer
*Dahlem Center for Complex Quantum Systems and Institut für Theoretische Physik,
 Freie Universität Berlin, D-14195, Berlin, Germany*

(Dated: February 26th, 2014)

Weyl semimetals are paradigmatic topological gapless phases in three dimensions. We here address the effect of disorder on charge transport in Weyl semimetals. For a single Weyl node with energy at the degeneracy point and without interactions, theory predicts the existence of a critical disorder strength beyond which the density of states takes on a nonzero value. Predictions for the conductivity are divergent, however. In this work, we present a numerical study of transport properties for a disordered Weyl cone at zero energy. For weak disorder our results are consistent with an RG flow towards an attractive pseudoballistic fixed point with zero conductivity and a scale-independent conductance; for stronger disorder diffusive behavior is reached. We identify the Fano factor as a signature that discriminates between these two regimes.

Introduction.— Topological considerations not only can be used to describe and classify band insulators and superconductors [1, 2], they were also found to apply to gapless phases of matter [3–10]. Perhaps the best known example of a topologically nontrivial gapless band structure is that of graphene [11], which has four topologically protected band touchings. The paradigmatic example of a topological gapless phase in three dimensions is the Weyl semimetal [12–14], which features pairs of topologically protected gap closing points in its Brillouin zone. The dispersion in the vicinity of a single isotropic nodal point can be described by the effective Hamiltonian

$$H_0(\mathbf{k}) = \pm \hbar v \boldsymbol{\sigma} \cdot \mathbf{k}, \quad (1)$$

where v is the Fermi velocity, $\boldsymbol{\sigma}$ the vector of Pauli matrices, \pm denotes the helicity, and \mathbf{k} measures the Bloch wavevector relative to the momentum in the Brillouin zone at which the gap closing appears.

Weyl semimetals have attracted considerable attention due to the prediction of protected surface states with a Fermi arc [13] and the chiral anomaly in electromagnetic response [15]. An ideal Weyl semimetal with Fermi energy at the Weyl point $\varepsilon = 0$ has a vanishing conductivity σ , but a finite conductance [16], making it neither conducting nor insulating. The excitement is further fueled by the existence of concrete theoretical proposals for material candidates for Weyl semimetals [13, 17, 18], as well as the experimental identification of “Dirac semimetals” [19–21], which have a pair of Weyl nodes forced to overlap by time-reversal and inversion symmetry. Although spectroscopic confirmation of a Weyl node in a real material has not yet been reported, specific magnetotransport signatures of Weyl nodes have been found in *BiSb* [22].

An important question that concerns the comparison of theory and experimental realizations is about the stability of the Weyl nodes to the presence of disorder [23]. This question is of particular fundamental interest if the disorder is sufficiently smooth that scattering between different Weyl nodes is avoided, since disorder that does not satisfy this condition immediately removes any topo-

logical protection and leads to a trivial gapping of the spectrum and/or localization of the wavefunctions.

In the theoretical literature, the study of the effect of disorder on a single Weyl node, without inclusion of electron-electron interactions, goes back to the mid 1980s [24, 25]. Far away from the Weyl point the expected behavior resembles that of normal metals: Disorder leads to diffusive dynamics, with a conductivity σ that decreases with increasing disorder strength. However, unlike a normal metal, a Weyl semimetal has no transition into an Anderson-localized phase in the limit of strong disorder [26]. Exactly at the Weyl point $\varepsilon = 0$ a completely different picture emerges: There is consensus that weak disorder is irrelevant [24, 25, 27, 28], so that the vanishing density of states $\nu(\varepsilon) \propto \varepsilon^2$ of the Hamiltonian (1) is maintained at finite disorder strength [29–31]; For stronger disorder, a quantum phase transition takes place, beyond which $\nu(0)$ is finite. There is no consensus for the implications of this scenario for the conductivity σ , however. Using the self-consistent Born approximation (SCBA), Ominato and Koshino find $\sigma = 0$ up to the critical disorder strength, and a finite conductivity that increases for stronger disorder [30], whereas Syzranov *et al.* argue for the opposite behavior [28]: A finite conductivity that decreases with increasing disorder below a critical disorder strength, and zero conductivity beyond that point. Boltzmann theory also gives a Weyl-point conductivity that is a decreasing function of disorder strength, but there is no critical disorder strength and σ is finite throughout [27, 30, 32].

Remarkably, the question about the effect of disorder on a single Weyl node has never been put to the test numerically. Recently, similar physics has been investigated for a disordered Dirac semimetal employing diagonalization of a large tight binding model [33]. The extension of these results to a Weyl semimetal is problematic, however, because any tight binding model with a Weyl node inevitably comes with its opposite-helicity partner node [34], coupling to which cannot be fully avoided. Yet, resorting to a numerical test is particularly relevant in the

present case, because none of the theoretical methods applied in the analytical theory cited above is fully controlled at the Weyl point $\varepsilon = 0$ (see Ref. 28 for a critical discussion).

In this letter, we report numerical calculations of the transport properties of a single Weyl node in the presence of a random potential. We limit ourselves to transport at the Weyl point $\varepsilon = 0$, which is the energy at which the differences between a Weyl semimetal and a normal metal are most pronounced. The focus on the nodal point is not entirely academic: In contrast to the two-dimensional case (graphene or surface states of topological insulators), where unintended doping generically shifts the chemical potential μ away from the nodal point, in the bulk of three-dimensional Weyl semimetals $\mu = 0$ can be expected from stoichiometric filling of the energy bands [29].

Our results for the conductivity qualitatively confirm the predictions of the SCBA [30], although quantitatively the numerical results for the critical disorder strength and for the conductivity approximately differ by a factor two. In the weak-disorder phase the system is better characterized by its conductance, which is finite, than by its conductivity, which is zero within the accuracy of our calculations. A transport signature that is nonzero in both phases is the Fano factor F , the ratio of the shot-noise power and the conductance, which we show to be an excellent indicator to discriminate between the pseudo-ballistic transport of the weak-disorder phase and the diffusive transport of the strong-disorder phase.

Model and numerical method.— Our numerical procedure closely follows Refs. 35 and 36, which considered the effect of disorder on the conductivity of graphene. We consider a Weyl semimetal of length $0 < x < L$ and transverse dimensions $0 < y, z < W$ with Hamiltonian

$$H = H_0 + U(\mathbf{r}) \quad (2)$$

where $U(\mathbf{r})$ is a Gaussian random potential with zero mean $\langle U_{\mathbf{q}} \rangle = 0$ and fluctuations

$$\langle U_{\mathbf{q}} U_{\mathbf{q}'}^* \rangle = \frac{K \xi \hbar^2 v^2}{W^2 L} e^{-q^2 \xi^2 / 2} \delta_{\mathbf{q}, \mathbf{q}'}, \quad (3)$$

where ξ is the correlation length and K the dimensionless disorder strength. A similar random potential has been used in studies of the Dirac equation in two dimensions [35]. For $x < 0$ and $x > L$ the Weyl semimetal is connected to ideal leads, which we model as Weyl semimetals with Hamiltonian $H_0 + V$, taking the limit $V \rightarrow -\infty$ [37]. We numerically compute the transmission matrix t at zero energy and determine the zero-temperature conductance using the Landauer formula $G(L, W) = (e^2/h) \text{tr} t t^\dagger$ and the Fano factor $F(L) = \text{tr} [t t^\dagger (1 - t t^\dagger)] / \text{tr} t t^\dagger$. To quantize transverse momenta and to eliminate a contribution from surface states, we apply periodic or anti-periodic boundary conditions in the y and z directions,

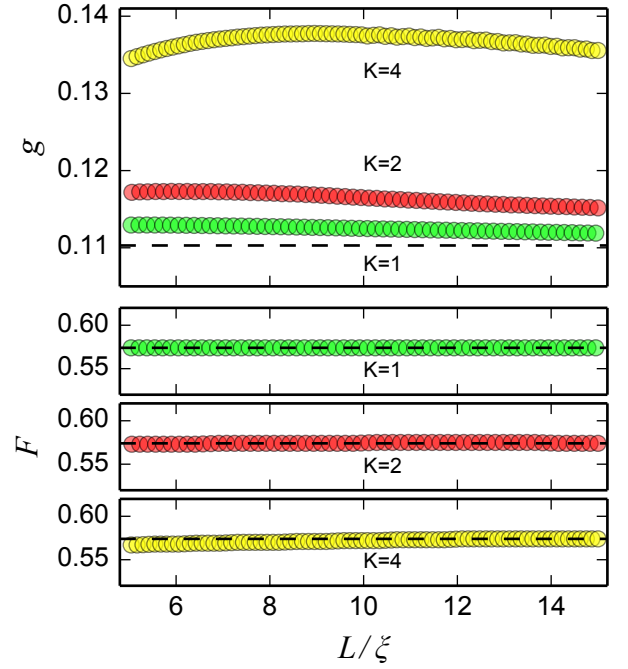


Figure 1. Dimensionless conductance g referred to a cubic sample of size L (top) and Fano factor F (bottom) for a single Weyl cone with a random potential for disorder strengths $K = 1, 2$, and 4 . The data represent a disorder average over at least 10 realizations. The dashed lines refer to the pseudoballistic limits g_0 and F_0 for an isotropic Weyl cone ($c = 1$).

and truncate at $|q_y|, |q_z| \leq 2M/\xi$, where we verified that the results do not depend on the cutoff M . To ensure bulk behavior, the width W is taken large enough that the results do not depend on the boundary conditions and the scaling $G \propto W^2$, F independent of W , holds.

Pseudoballistic regime.— For the low-disorder regime, we rescale the calculated conductance $G(L, W)$ to find the dimensionless conductance $g(L)$ of a cube with linear dimension L ,

$$G(L, W) = \frac{e^2 W^2}{h L^2} g(L). \quad (4)$$

In the absence of disorder g and the Fano factor F are independent of L [16], taking the values

$$g_0 = \frac{\ln 2}{2\pi} c, \quad F_0 = \frac{1}{3} + \frac{1}{6 \ln 2} \approx 0.574, \quad (5)$$

with c a numerical factor that takes the value $c = 1$ (so that $g_0 \approx 0.110$) for an isotropic Weyl cone. The results of numerical calculations of $g(L)$ and $F(L)$ for disorder strengths $K = 1, 2$, and 4 are shown in Fig. 1. The numerical data show that the presence of the random potential $U(\mathbf{r})$ leads to a bulk conductance g that is always larger than the pseudoballistic value g_0 , but also that the conductance $g(L)$ is a bounded function of L

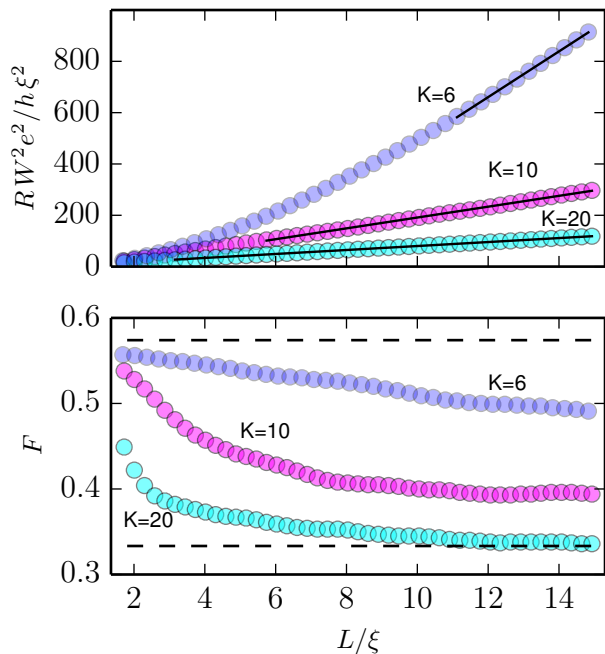


Figure 2. Resistance R (top) and Fano factor F (bottom) for a single Weyl cone vs. system length L , for disorder strengths $K = 6, 10$, and 20 . The thin solid lines indicate the linear fit for the conductivity σ . The dashed lines refer to the pseudoballistic and diffusive limits for the Fano factor F . The data represent a disorder average over at least 35 realizations.

and monotonically decreases in the large- L limit. For the system sizes within our reach this decrease is most pronounced for weak disorder ($K = 1$), and less pronounced for stronger disorder ($K = 4$), consistent with the theoretical expectation that weak disorder is an irrelevant perturbation at $\varepsilon = 0$ [27, 28]. The fact that $g(L)$ remains bounded as a function of L is consistent with a vanishing conductivity $\sigma = 0$. (A finite conductivity would correspond to $g(L) \propto L$.) The Fano factor F takes the pseudoballistic value F_0 for all system sizes considered.

It should be emphasized that the absence of a conductivity is a property special to the Weyl point $\varepsilon = 0$. At $\varepsilon \neq 0$ the conductivity σ diverges at $K = 0$, and one expects a finite conductivity at finite disorder strengths [17, 29, 30]. This finite conductivity away from the Weyl point also dominates the Weyl point conductivity at finite temperature [29]. Hence, in order to bring out the anomalous transport properties characteristic of the Weyl point in the pseudoballistic regime, the zero temperature limit is essential.

Diffusive regime.— For stronger disorder, the conductivity σ becomes finite. Although σ can in principle be obtained from the conductance using the relation $G(L, W) = \sigma W^2/L$, we employ a slightly different procedure to obtain σ from the numerically calculated conductance $G(L, W)$, in order to eliminate the ef-

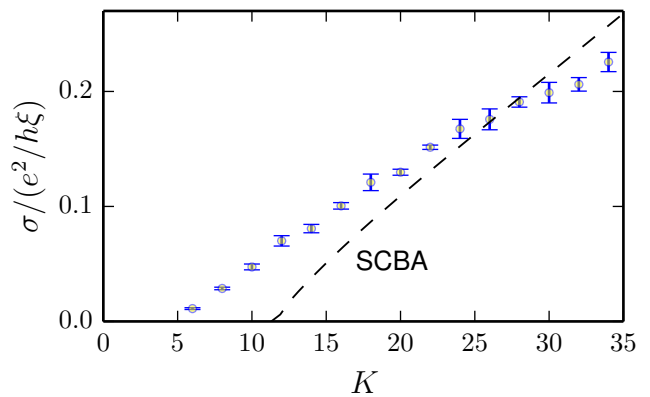


Figure 3. Conductivity σ for disordered Weyl cone as a function of the disorder strength K . The data represent a disorder average over at least 20 disorder realizations. The dashed line refers to the SCBA theory of Ref. 30.

fect of a finite contact resistance. Figure 2 shows the resistance $R(L, W) = 1/G(L, W)$ and the Fano factor $F(L)$ as a function of length L , for disorder strengths $K = 6, 10$ and 20 . In the diffusive regime, one expects $R(L, W) \propto L/W^2\sigma$, so that the conductivity can be calculated as $\sigma^{-1} = W^2\partial R/\partial L$. We indeed observe a linear R vs. L dependence for L sufficiently large. The Fano factor F takes the diffusive value $F = 1/3$ for large L for the stronger disorder strengths such as $K = 20$. For $K = 6$ and $K = 10$ the Fano factor F is below the pseudoballistic limit and decreases with increasing L , but no limiting value could be determined for the system sizes available in our calculations. The dependence of the conductivity σ on disorder strength K is summarized in Fig. 3. We estimate that the conductivity is nonzero above a critical disorder $K_c \approx 5$, the behavior for K just above K_c being consistent with a linear increase $\propto K - K_c$ [25, 30]; Finite-size effects prohibit a more accurate determination of the critical disorder strength. Although we adopted the expression “critical disorder strength”, we note that our numerical analysis does not allow us to determine the precise nature of the transition. In passing, we also note that the conductance distribution is widest around K_c (data not shown), a behavior well known from the three-dimensional Anderson phase transition [38].

A recent work by Ominato and Koshino [30] calculates the Weyl-point conductivity σ using the SCBA but without further approximations, employing a correlated disorder potential compatible with the random potential used in the present numerical simulation. Relating the impurity model of Ref. [30] to our Gaussian model we find a theoretical value $K_c^{\text{SCBA}} \approx 11.3$ and a conductivity as shown by the dashed line Fig. 3 [39]. Both the value of K_c^{SCBA} and the slope of the SCBA conductivity vs. disorder strength K are roughly off by a factor of two from the numerical results.

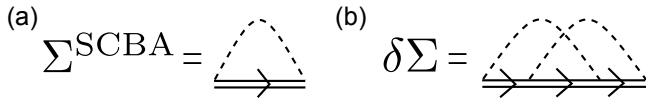


Figure 4. Diagrammatic representation of the SCBA self energy Σ^{SCBA} (a) and the leading correction $\delta\Sigma$ (b). The double solid lines denote the SCBA propagator; dashed lines are disorder correlators.

In order to understand the quantitative failure of the SCBA we have analyzed the corrections to the SCBA result for the self energy $\Sigma(\mathbf{k}, \omega)$, which is related to the single-particle Green function $\mathcal{G}(\mathbf{k}, \omega)$ through the standard relation $\mathcal{G}(\mathbf{k}, \omega) = [\omega - H_0 - \Sigma(\mathbf{k}, \omega)]^{-1}$. The diagrammatic expression for $\Sigma(k, \omega)$ in the SCBA is shown in Fig. 4(a), where the double lines denote the single-particle Green function \mathcal{G} with Σ replaced by Σ^{SCBA} . Figure 4(b) contains the leading correction $\delta\Sigma$ to Σ^{SCBA} . The consistency of the SCBA requires that $\delta\Sigma$ is parametrically smaller than Σ^{SCBA} . Indeed, for a standard disordered metal one finds $\delta\Sigma/\Sigma^{\text{SCBA}} = \mathcal{O}(1/k_F l)$ [40], where k_F is the Fermi wavevector and l the mean free path.

For the Weyl semimetal at zero energy one has $k_F = 0$ and this standard argument does not apply. We have calculated the leading correction $\delta\Sigma$ at $k = 0$ and $\omega = 0$ using a simplified model for the disorder potential [30], in which the Gaussian correlator (3) is replaced by a cutoff at $q = 2/\xi$,

$$\langle U_{\mathbf{q}} U_{\mathbf{q}'}^* \rangle = \frac{K' \xi \hbar^2 v^2}{W^2 L} \Theta(2/\xi - q) \delta_{\mathbf{q}, \mathbf{q}'}. \quad (6)$$

In this simplified model one has the critical disorder strength $K'_c = \pi^2$ and the SCBA self energy $\Sigma(0, 0)^{\text{SCBA}} = (4\pi i \hbar v / \xi)(1/K' - 1/K'_c) \Theta(K' - K'_c)$ [30]. Calculation of the diagram of Fig. 4(b) for K' close to the critical disorder strength K'_c then gives [41]

$$\frac{\delta\Sigma(0, 0)}{\Sigma(0, 0)^{\text{SCBA}}} \simeq 0.62 + 11 \left(\frac{1}{K'_c} - \frac{1}{K'} \right), \quad (7)$$

which is not parametrically small. Since the simplified model (6) does not qualitatively differ from the Gaussian model used in the numerical calculations [30], we expect that this result carries over to that case, too.

Discussion.— In the framework of Drude transport theory, the quasiparticles at the Fermi energy are endowed with a mean free path, which becomes shorter if the disorder becomes stronger. At the same time, the presence of a random impurity potential has negligible effect on the density of states. The result is a conductivity that decreases upon increasing the disorder strength. For a Weyl node at the degeneracy point it is the disorder which generates the density of states [24, 25, 27–30],

a finite density of states appearing only above a certain critical disorder strength. As a result of this vastly different physical mechanism, a Weyl node at the degeneracy point shows behavior opposite to that of a normal metal: increasing disorder typically leads to an increase of the conductivity [30]. This remarkable theoretical prediction has been confirmed in our numerical calculations.

The increase in conductivity with disorder is reminiscent of the two-dimensional Dirac Hamiltonian $H_0^{2d} \propto v(k_x \sigma_x + k_y \sigma_y)$, for which the conductivity σ was also found to be an increasing function of disorder strength [35, 36, 42]. A fundamental difference with graphene is, however, that graphene has a finite conductivity for all disorder strengths, whereas the Weyl semimetal at the degeneracy point requires a minimum disorder strength for diffusive behavior to set in.

For the two-dimensional Dirac Hamiltonian, the inverted dependence of conductivity on disorder strength was found to be related to the fact that H_0^{2d} (with a disorder term but without the condition that the disorder be smooth, because of the absence of other Dirac nodes) is the surface theory of a three-dimensional time-reversal invariant topological insulator [26]. Similarly, the surface theory of a hypothetical four-dimensional topological insulator is described by the Hamiltonian H_0 of Eq. (1). Thus, it is expected on general grounds that H_0 evades localization [26]. Our numerical results are consistent with this expectation. Indeed, although the conductivity σ vanishes in the weak-disorder regime, the conductance g remains finite. It is a finite conductance, not a finite conductivity, which is the proper signature of absence of localization [43].

Our numerical calculations have shown that the conductance g and the Fano factor F contain important additional information that is not contained in the conductivity σ . This is particularly relevant for the pseudobalistic weak disorder regime, where σ vanishes, whereas g and F take on nonzero values. A three-dimensional phase with a finite scale-independent bulk conductance is known from the Anderson metal-insulator transition, where it occurs at the critical disorder strength. A crucial difference of the pseudobalistic phase at the Weyl point is that its scale-independent conductance represents an attractive fixpoint, which requires no fine tuning of disorder strength.

Acknowledgments.— We acknowledge helpful discussions with Georg Schwiete and Martin Schneider and we thank Jörg Behrmann for support with the computations. Financial support was granted by the Helmholtz Virtual Institute “New states of matter and their excitations”, by the Alexander von Humboldt Foundation in the framework of the Alexander von Humboldt Professorship, endowed by the Federal Ministry of Education and Research, and by DFG’s Emmy Noether program (BE 5233/1-1).

-
- [1] M. Z. Hasan and C. L. Kane, Rev. Mod. Phys. **82**, 3045 (2010).
- [2] B. A. Bernevig, *Topological Insulators and Topological Superconductors* (Princeton University Press, 2013).
- [3] X. G. Wen and A. Zee, Phys. Rev. B **66**, 235110 (2002).
- [4] P. Hořava, Phys. Rev. Lett. **95**, 016405 (2005).
- [5] M. Sato, Phys. Rev. B **73**, 214502 (2006).
- [6] B. Béri, Phys. Rev. B **81**, 134515 (2010).
- [7] G. Volovik, JETP Letters **93**, 66 (2011).
- [8] D. Bernard, E.-A. Kim, and A. LeClair, Phys. Rev. B **86**, 205116 (2012).
- [9] Y. X. Zhao and Z. D. Wang, Phys. Rev. Lett. **110**, 240404 (2013).
- [10] S. Matsuura, P.-Y. Chang, A. P. Schnyder, and S. Ryu, New J. Phys. **15**, 065001 (2013).
- [11] P. R. Wallace, Phys. Rev. **71**, 622 (1947).
- [12] S. Murakami, New J. Phys. **356** (2007).
- [13] X. Wan, A. M. Turner, A. Vishwanath, and S. Y. Savrasov, Phys. Rev. B **83**, 205101 (2011).
- [14] For a review see P. Hosur and X. Qi, C. R. Physique **14**, 857 (2013).
- [15] M. M. Vazifeh and M. Franz, Phys. Rev. Lett. **111**, 027201 (2013).
- [16] P. Baireuther, J. M. Edge, I. C. Fulga, C. W. J. Beenakker, and J. Tworzydło, Phys. Rev. B **89**, 035410 (2014).
- [17] A. A. Burkov and L. Balents, Phys. Rev. Lett. **107**, 127205 (2011).
- [18] D. Bulmash, C.-X. Liu, and X.-L. Qi, Phys. Rev. B **89** (2014).
- [19] M. Neupane, S. Xu, R. Sankar, N. Alidoust, G. Bian, C. Liu, I. Belopolski, T. Chang, H. Jeng, H. Lin, A. Bansil, F. Chou, and M. Z. Hasan, arXiv:1309.7892v1 (2013).
- [20] S. Borisenko and Q. Gibson, arXiv:1309.7978v1 (2013).
- [21] Z. K. Liu, B. Zhou, Y. Zhang, Z. J. Wang, H. M. Weng, D. Prabhakaran, S.-K. Mo, Z. X. Shen, Z. Fang, X. Dai, Z. Hussain, and Y. L. Chen, Science **343**, 864 (2014).
- [22] H.-J. Kim, K.-S. Kim, J.-F. Wang, M. Sasaki, N. Satoh, A. Ohnishi, M. Kitaura, M. Yang, and L. Li, Phys. Rev. Lett. **111**, 246603 (2013).
- [23] The effect of a single impurity on the electronic structure of a Weyl node has been studied recently in Z. Huang, T. Das, A. Balatsky, and D. Arovas, Phys. Rev. B **87**, 155123 (2013).
- [24] E. Fradkin, Phys. Rev. B **33**, 3257 (1986).
- [25] E. Fradkin, Phys. Rev. B **33**, 3263 (1986).
- [26] S. Ryu, A. P. Schnyder, A. Furusaki, and A. W. W. Ludwig, New J. Phys. **12**, 065010 (2010).
- [27] A. A. Burkov, M. D. Hook, and L. Balents, Phys. Rev. B **84**, 235126 (2011).
- [28] S. V. Syzranov, L. Radzihovsky, and V. Gurarie, arxiv:1402.3737 (2014).
- [29] R. R. Biswas and S. Ryu, Phys. Rev. B **89**, 014205 (2014).
- [30] Y. Ominato and M. Koshino, arXiv:1309.4206v2 (2013).
- [31] R. Nandkishore, D. Huse, and S. Sondhi, arXiv:1307.3252v2 argue that a finite density of states arises from rare-region effects even below the critical disorder strength.
- [32] P. Hosur, S. A. Parameswaran, and A. Vishwanath, Phys. Rev. Lett. **108**, 046602 (2012).
- [33] K. Kobayashi, T. Ohtsuki, K.-I. Imura, and I. F. Herbut, Phys. Rev. Lett. **112**, 016402 (2014).
- [34] H. Nielsen and M. Ninomiya, Nucl. Phys. B **185**, 20 (1981).
- [35] J. H. Bardarson, J. Tworzydło, P. W. Brouwer, and C. W. J. Beenakker, Phys. Rev. Lett. **99**, 106801 (2007).
- [36] S. Adam, P. W. Brouwer, and S. Das Sarma, Phys. Rev. B **79**, 201404 (2009).
- [37] J. Tworzydło, B. Trauzettel, M. Titov, A. Rycerz, and C. W. J. Beenakker, Phys. Rev. Lett. **96**, 246802 (2006).
- [38] K. Slevin and T. Ohtsuki, Phys. Rev. Lett. **78**, 4083 (1997).
- [39] The theory of Ref. 30 can be applied to our calculations by making the substitutions $d_0 \leftrightarrow \xi$ and $W \leftrightarrow K/2\pi$.
- [40] J. Rammer, *Quantum Transport Theory* (Perseus Books, 1998).
- [41] Details of this calculation are given in the appendix.
- [42] S. Das Sarma, E. H. Hwang, and Q. Li, Phys. Rev. B **85**, 195451 (2012).
- [43] Y. Imry, *Introduction to mesoscopic physics* (Oxford University Press, 2002).

APPENDIX: LEADING CORRECTION TO SCBA SELF ENERGY

We compute the leading correction $\delta\Sigma$ to the SCBA self energy Σ^{SCBA} at zero momentum $\mathbf{k} = 0$ and zero energy $\omega = 0$. The diagrammatic representation for the correction $\delta\Sigma(\mathbf{k}, \omega)$ is shown in Fig. 4(b),

$$\delta\Sigma(\mathbf{k}, \omega) = \sum_{\mathbf{k}_1, \mathbf{k}_2} \mathcal{G}(\mathbf{k} + \mathbf{k}_1, \omega) \mathcal{G}(\mathbf{k} + \mathbf{k}_1 + \mathbf{k}_2, \omega) \mathcal{G}(\mathbf{k} + \mathbf{k}_2, \omega) \langle |U_{\mathbf{k}_1}|^2 \rangle \langle |U_{\mathbf{k}_2}|^2 \rangle, \quad (8)$$

where $\mathcal{G}(\mathbf{k}, \omega) = [\omega - H_0 - \Sigma(\mathbf{k}, \omega)^{\text{SCBA}}]^{-1}$ is the SCBA propagator and U the disorder potential. Taking the disorder correlator $\langle |U_{\mathbf{k}}|^2 \rangle$ from Eq. (6), setting $\mathbf{k} = 0$, $\omega = 0$, and replacing the summation over \mathbf{k}_1 and \mathbf{k}_2 by an integration one finds

$$\delta\Sigma(0, 0) = K'^2 \xi^2 (\hbar v)^4 \int_{k_1 < 2/\xi} \frac{d\mathbf{k}_1}{(2\pi)^3} \int_{k_2 < 2/\xi} \frac{d\mathbf{k}_2}{(2\pi)^3} \mathcal{G}(\mathbf{k}_2, 0) \mathcal{G}(\mathbf{k}_1 + \mathbf{k}_2, 0) \mathcal{G}(\mathbf{k}_1, 0).$$

Employing the identity $(a - \mathbf{b} \cdot \boldsymbol{\sigma})^{-1} = (a + \mathbf{b} \cdot \boldsymbol{\sigma})/(a^2 - |\mathbf{b}|^2)$ and substituting [30]

$$\Sigma(0, 0)^{\text{SCBA}} = \frac{4\pi i \hbar v}{\tilde{K}' \xi}, \quad \tilde{K}' = \frac{1}{1/K' - 1/K'_c}, \quad (9)$$

for disorder strength $K' > K'_c$, one finds that (for a positive helicity Weyl node) the single-particle propagator \mathcal{G} is given by the expression

$$\mathcal{G}(\mathbf{k}, 0) = \left(\frac{\xi}{2\hbar v} \right) \frac{(2\pi/\tilde{K}')i - (\xi/2)\mathbf{k} \cdot \boldsymbol{\sigma}}{(2\pi/\tilde{K}')^2 + (\xi/2)^2 k^2}. \quad (10)$$

Switching to the dimensionless variables $\mathbf{x}_{1,2} = \mathbf{k}_{1,2}\xi/2$ we arrive at

$$\begin{aligned} \frac{\delta\Sigma(0, 0)}{\Sigma(0, 0)^{\text{SCBA}}} &= \frac{K'^2 \tilde{K}'}{32\pi^7 i} \\ &\times \int_{x_1 < 1} d\mathbf{x}_1 \int_{x_2 < 1} d\mathbf{x}_2 \left(\frac{2\pi i/\tilde{K}' - \mathbf{x}_2 \cdot \boldsymbol{\sigma}}{(2\pi/\tilde{K}')^2 + x_2^2} \right) \left(\frac{2\pi i/\tilde{K}' - (\mathbf{x}_1 + \mathbf{x}_2) \cdot \boldsymbol{\sigma}}{(2\pi/\tilde{K}')^2 + |\mathbf{x}_1 + \mathbf{x}_2|^2} \right) \left(\frac{2\pi i/\tilde{K}' - \mathbf{x}_1 \cdot \boldsymbol{\sigma}}{(2\pi/\tilde{K}')^2 + x_1^2} \right). \end{aligned} \quad (11)$$

Finally, after introducing polar coordinates for the integrations over \mathbf{x}_1 and \mathbf{x}_2 one finds after some standard manipulations

$$\begin{aligned} \frac{\delta\Sigma(0, 0)}{\Sigma(0, 0)^{\text{SCBA}}} &= \frac{K'^2}{4\pi^4} \int_0^1 dx_1 \int_0^1 dx_2 \frac{x_1^2 x_2^2}{[(2\pi/\tilde{K}')^2 + x_1^2][(2\pi/\tilde{K}')^2 + x_2^2]} \left\{ 6 - \left[\frac{5}{2}(2\pi/\tilde{K}')^2 + \frac{1}{2}(x_1^2 + x_2^2) \right] \right. \\ &\times \left. \int_0^\pi d\zeta \int_\zeta^\pi d\theta \frac{\cos \zeta - \cos \theta}{\sqrt{[(2\pi/\tilde{K}')^2 + x_1^2 + x_2^2 + 2x_1 x_2 \cos \zeta][(2\pi/\tilde{K}')^2 + x_1^2 + x_2^2 + 2x_1 x_2 \cos \theta]}} \right\}. \end{aligned} \quad (12)$$

Numerical evaluation of the fourfold integral for K' in the vicinity of the critical disorder strength K'_c then results in the estimate (7) quoted in the main text.